Surface-Enhanced Vibrational Spectroelectrochemistry: Electric-Field Effects on Redox and Redox-Coupled Processes of Heme Proteins

Daniel Murgida and Peter Hildebrandt

Technische Universität Berlin, Institut für Chemie, Max-Volmer-Laboratorium für Biophysikalische Chemie, Sekr. PC14, Strasse des 17. Juni 135, D-10623 Berlin, Germany
dh.murgida@tu-berlin.de, hildebrandt@chem.tu-berlin.de

1 Introduction

Soon after its discovery, the surface-enhanced Raman (SER) effect was exploited to study adsorbed biomolecules including proteins and nucleic acids [1, 2]. In their pioneering work on heme proteins adsorbed on Ag electrodes, *Van Duyne* and *Cotton* demonstrated that the SER effect and the molecular resonance Raman (RR) effect can be combined (surface-enhanced resonance Raman SERR) to selectively probe the protein cofactor [1]. Although at that time the origin of the surface enhancement was far from being fully understood, SER spectroscopy was proposed to become a valuable tool in studying biological systems. This optimistic view, however, was damped by later findings on adsorption-induced denaturation of proteins [3, 4], casting serious doubts on the general applicability of this technique to study biological systems.

It took eventually more than fifteen years to establish strategies that are appropriate to overcome this problem. Using biocompatible coatings of the metal surface now allows immobilization of proteins under preservations of their native structure [5, 6]. Additional methodological achievements including the development of time-resolved SERR spectroscopy [7, 8, 9] as well as the application of surface-enhanced infrared absorption spectroscopy (SEIRA) [10] have substantially broadened the scope and the potential of studies on immobilized proteins.

This account is dedicated to summarize recent results on the redox processes of heme proteins on coated electrodes using potential-dependent stationary and time-resolved SER, SERR and SEIRA spectroscopy. The first part of this work is devoted to outline various strategies for immobilizing proteins on metal electrodes, the adaptation of stationary and time-resolved surface-enhanced vibrational spectroscopic techniques to biological systems, and the control and determination of the interfacial electric-field. In the second and third parts, we summarize results obtained for proteins peripherally bound to and integrated in membrane models on electrodes. Special empha-

K. Kneipp, M. Moskovits, H. Kneipp (Eds.): Surface-Enhanced Raman Scattering – Physics and Applications, Topics Appl. Phys. **103**, 313–334 (2006)

sis is laid on electric-field effects on redox and redox-coupled processes of immobilized cytochrome *c* and cytochrome *c* oxidase.

2 Strategy and Methodological Approach

The analysis of electric-field effects on interfacial processes of heme proteins requires, first, an appropriate strategy to immobilize proteins that provides a biomimetic environment and avoids irreversible denaturation (Sect. 2.1). Second, surface-enhanced vibrational spectroscopic techniques have to be adapted to the investigation of sensitive biological materials such that proteins are not degraded during the experiments. Moreover, the techniques must be capable of providing information about the structure and the dynamics of the adsorbed species (Sect. 2.2). Third, the devices must allow a controlled variation and the quantification of the electric-field strength (Sect. 2.3).

2.1 Protein Immobilization on SER/SEIRA Active Metal Electrodes

The most widespread approach for biocompatible coating of SER/SEIRA-active electrodes is based on the chemisorption of ω-functionalized alkanethiols or disulfides on Ag and Au surfaces [5,6]. Depending on their chain length and ω-substituents, these compounds can form densely packed self-assembled monolayers (SAMs) that have very negative potentials of reductive desorption (typically $< -0.6\,\mathrm{V}$ vs. NHE) [11, 12, 13, 14]. The potential window for SER/SERR and SEIRA studies is, however, narrowed by reversible or irreversible potential-dependent phase transitions depending on the specific SAM [15].

The chemical variability of the SAM tail groups provides the basis for different modes of protein immobilization, particularly suitable for soluble proteins. Proteins having cationic or anionic binding domains can form stable electrostatic complexes with SAMs that contain acidic or basic tail groups, e.g., $-CO_2H$, $-PO_4H_3$, or $-NH_2$ [5,6,11,12,14,16,17,18,19,20]. Electrostatic adsorption is particularly useful for proteins with a high molecular dipole moment that leads to a largely uniform orientation. NH_2- or COOH-terminated SAMs also serve as a starting point for covalent attachment by crosslinking to anionic or cationic amino acid side chains through carbodiimide reagents [21]. In this case, however, one usually obtains a broader distribution of orientations depending on the reactivity of the individual amino acid side chains. Alternatively, proteins can be crosslinked to the SAM via cysteines, which, if required, have to be introduced to the protein surface by site-directed mutagenesis. The thiol side chain can then be bound to NH_2-terminated SAMs previously treated with N-succinimidyl iodoacetate or N-β-maleimidopropionic acid and carbodiimide. Crosslinking of cysteine residues to OH-terminated SAMs is also possible using N-(p-maleimidophenyl)-isocyanate.

Using methyl-terminated SAMs, hydrophobic interactions also may allow a firm immobilization as has been demonstrated for cytochrome c (Cyt-c) [22] and azurin [11, 23]. Mixed monolayers containing protonable, hydrophobic and/or polar tail groups can also be constructed, although lateral phase separation may be difficult to avoid. In some cases, the redox center of the protein can be directly wired to the electrode using SAMs with tail groups that are capable of coordinating to the cofactor such as to the heme group in Cyt-c [24,25,26], or that may serve as a cofactor such as the flavin group in glucose oxidase [27]. In addition to the rather well-ordered SAMs, electrodes can be coated with polyelectrolytes or clays that allow for the embedment of proteins in relatively large quantities, albeit not in a uniform orientation [28, 29, 30].

Membrane proteins represent a special case since they require a hydrophobic environment that mimics the membrane core as a prerequisite for maintaining the native structure and avoiding protein aggregation. This requirement can be fulfilled either by solubilization in detergents or by reconstitution in phospholipid bilayers. Thus, the simplest approach for immobilizing membrane proteins consists in the direct adsorption of the detergent-solubilized protein onto the metal surface. This strategy has been recently employed for the immobilization of the heme-Cu quinol oxidase from *Acidianus ambivalens* on Ag electrodes coated with specifically adsorbed phosphate anions [31]. It was shown that, under the specific conditions of that study, adsorption occurs without displacement of the detergent, which then provides a biocompatible interface. Albeit straightforward, this mode of immobilization may lead to a distribution of different enzyme orientations. Alternatively, protein-containing lipid bilayers can be deposited on solid supports using Langmuir–Blodgett methods [32]. More recently, various types of solid-supported lipid bilayer membranes have been developed, including bilayers floating freely on quartz, indium tin oxide or gold surfaces, as well as polymer-, polyelectrolyte-supported and tethered bilayer lipid membranes, and some of these devices have been successfully employed in SERR and SEIRA spectroscopic studies [33, 34, 35, 36, 37, 38].

One of the most elegant approaches is based on binding the solubilized protein via a histidine tag (his-tag) to the electrode coated with Ni (or Zn) nitrilo triacetate (Ni–NTA). The high affinity of the Ni–NTA monolayer towards the his-tag guarantees a large surface coverage of uniformly oriented proteins even at the relatively high ionic strengths encountered under physiological conditions. The immobilized enzyme is then incubated in the presence of lipids and biobeads in order to remove the solubilizing detergent and allow the formation of a lipid bilayer. This method has been successfully applied for immobilization of cytochrome c oxidase (CcO) on Ag and Au electrodes [34, 36].

2.2 Surface-Enhanced Vibrational Spectroelectrochemistry of Heme Proteins

The electronic absorption spectrum of porphyrins is characterized by an intense band at ca. 410 nm (Soret band) and a weaker band at ca. 550 nm (Q band). Excitation in resonance with these transitions leads to a strong and selective enhancement of the Raman-active modes of the porphyrin such that the RR spectrum of a heme protein exclusively displays vibrational bands of the heme, regardless of the size of the optically transparent protein matrix. Due to the relatively high symmetry of the heme, which to a first approximation can be considered as D_{4h}, excitation in resonance with the allowed Soret and the forbidden Q band leads to specific enhancement patterns. Upon Soret-band excitation, the RR spectrum is dominated by the totally symmetric A_{1g} modes of the porphyrin, and displays those bands that are particularly diagnostic for specific structural properties of the porphyrin such as the oxidation, spin, and ligation state of the heme iron ("marker bands"; 1300 cm^{-1} to 1700 cm^{-1}) and the interactions of the heme with the surrounding protein ("fingerprint"; 200 cm^{-1} to 500 cm^{-1}) [39, 40]. For this reason and due to the distinctly larger resonance enhancement, Soret-band excitation is usually preferred compared to Q-band excitation.

When the protein is immobilized on SER-active metal surfaces RR and SER combine (SERR), provided that laser excitation simultaneously meets the resonance conditions of the electronic transition of the heme and the surface plasmons of the metal. This condition can only be fulfilled for Ag surfaces that exhibit maximum surface enhancement typically at ca. 500 nm. The highest SERR intensity is obtained with 413 nm or 407 nm excitation since the strong molecular RR enhancement clearly overrides the poorer surface enhancement in the violet region as compared to Q-band excitation at ca. 550 nm (strong SER, but low RR). Indeed, Soret-band excitation yields SERR signals of good quality even for heme proteins that are separated from the metal surface by spacers of up to 5 nm thickness [35, 37].

The SERR spectra that are obtained in this way allow different states of oxidation, spin and coordination of the heme iron [5, 6] to be distinguished. For instance, the SERR spectra of Cyt-c electrostatically immobilized on SAMs of mercaptohexadecanoic acid exclusively display the characteristic band patterns of the reduced and oxidized forms when measured 100 mV below and above the redox potential, respectively (Figs. 1a,b) [41].

Band positions and intensities of the ferrous and ferric form are sufficiently different to allow for quantitative spectral component analysis of redox mixtures. In this analysis, the complete spectra of the individual components are fitted to the experimental spectra of the mixture varying only the relative contributions of the component spectra [42]. The method is also applicable for spectra involving additional components such as those in which the heme iron exhibits different spin configurations and coordination patterns (Figs. 1c,d). On the basis of the component analysis, thermodynamic constants of redox

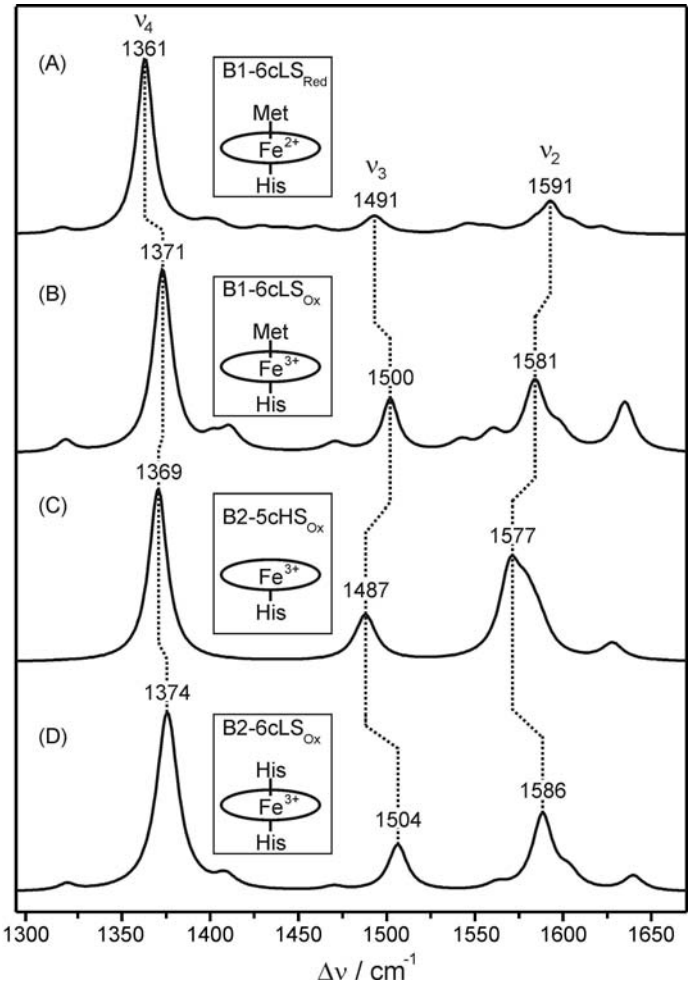

Fig. 1. SERR spectra of Cyt-c in different redox, coordination and spin states

and conformational equilibria of adsorbed heme proteins can be evaluated from potential-dependent SERR measurements as is illustrated in Fig. 2a.

SERR spectroelectrochemistry can be operated in the time-resolved (TR) mode by synchronizing fast potential jumps with short measuring events [6, 7, 9]. The most versatile TR SERR approach is based on electro-optically gated continuous wave (cw) excitation that generates laser pulses of low photon flux and variable duration down to the long nanoseconds timescale. These pulses define the measurement intervals that follow the potential jump after a variable delay time δ (Fig. 3). Subsequent to the measurement interval, the electrode potential is reset to the initial value to restore the original equilibrium. The sequence of potential jumps, delay times, and measurement

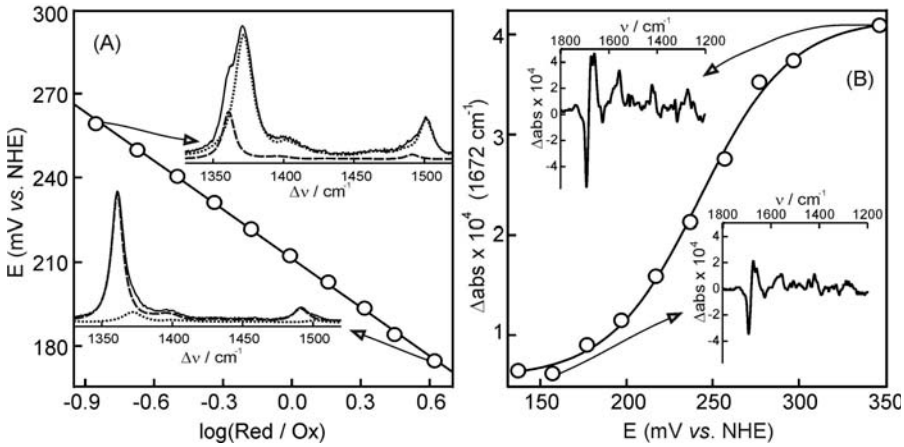

Fig. 2. Redox titrations of Cyt-c electrostatically adsorbed on a COOH-terminated SAM. (**a**) Nernstian plot based on potential-dependent SERR measurements. The *insets* show the experimental SERR spectra at two selected potentials with the reduced and oxidized components represented in *dashed* and *dotted lines*, respectively. (**b**) SEIRA titration curve based on the potential dependence of the amplitude of the 1672 cm^{-1} band with respect to a reference potential of 100 mV. The *insets* show the difference SEIRA spectra at two selected potentials

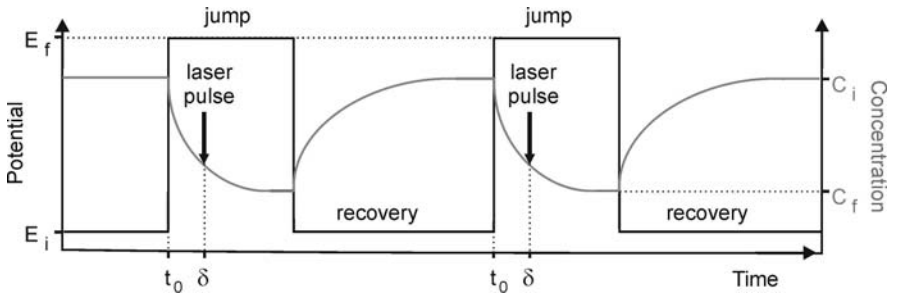

Fig. 3. Schematic representation of a TR SERR measurement. The sequence of potential jumps is represented with *black lines* and the corresponding variation of concentrations is indicated in *gray*

intervals, which are synchronized by a pulse delay generator, is repeated until the signal accumulated on a low-noise CCD detector of the spectrograph is of sufficient quality. A prerequisite for this approach is the full reversibility of the potential-dependent processes. The temporal resolution is mainly limited by the response time of the electrochemical cell, which is usually within a few tens of microseconds.

The main advantage of SERR spectroelectrochemistry, compared to conventional electrochemical techniques, is that it allows identifying and moni-

toring the molecular structures of the species that are involved in the interfacial redox reactions. This is particularly important for complex interfacial redox processes that involve various redox sites (e.g., multiheme proteins) or that are coupled to non-Faradaic processes. The main drawback of the method is that the SER effect is limited to microscopically roughened surfaces and only to a few metals, particularly Ag and Au. Laser-induced damage of the adsorbed proteins due to local heating or photochemical processes may also impose severe limitations. In most cases the damage can be avoided or minimized using low laser powers and continuous movement of the electrode surface with respect to the laser focus, for example using rotating electrodes [43, 44].

The information about the structure and dynamics of the adsorbed heme proteins that can be obtained by SERR spectroscopy is restricted to the redox site. To also probe structural changes of the protein matrix, SEIRA spectroscopy has to be employed. This technique traces spectral changes of the entire protein, specifically of the amide I modes that are sensitive indicators of the secondary structure. SEIRA measurements are most conveniently combined with the attenuated total reflection (ATR) technique [10]. For that purpose, a silicon ATR crystal is covered with a thin layer of SAM-coated Au or Ag that serves as the working electrode such that in-situ measurements in an electrochemical cell are possible without significant interference by water bands. Residual contributions from the solvent are largely cancelled since SEIRA measurements are carried out in the difference mode, which also significantly simplifies the SEIRA spectra. Since the enhancement of the IR bands strongly depends on the orientation of underlying dipole moments as well as on the distance with respect to the electrode surface, the absolute SEIRA spectra do not necessarily reflect all IR-active bands of the protein. Thus, unlike conventional IR spectroscopy in solution, determination of the protein secondary structure is not possible in SEIRA spectroscopy. However, potential-dependent processes of the adsorbed protein can be studied by subtracting a spectrum obtained at a reference potential from each measured spectrum. The difference spectra exclusively display those bands that reflect potential-dependent structural and orientational changes of the immobilized protein (Fig. 2b). Time-resolved SEIRA measurements can be performed by operating the FTIR spectrometer in the step-scan or rapid scan modes to monitor the dynamics of the protein structural changes subsequent to a potential jump.

2.3 Theoretical Description and Experimental Determination of the Electric-Field

The surface coatings described in Sect. 2.1 provide a biocompatible environment for the immobilization of several proteins. In addition, they offer the possibility of controlling the electric-field strength at the protein binding site.

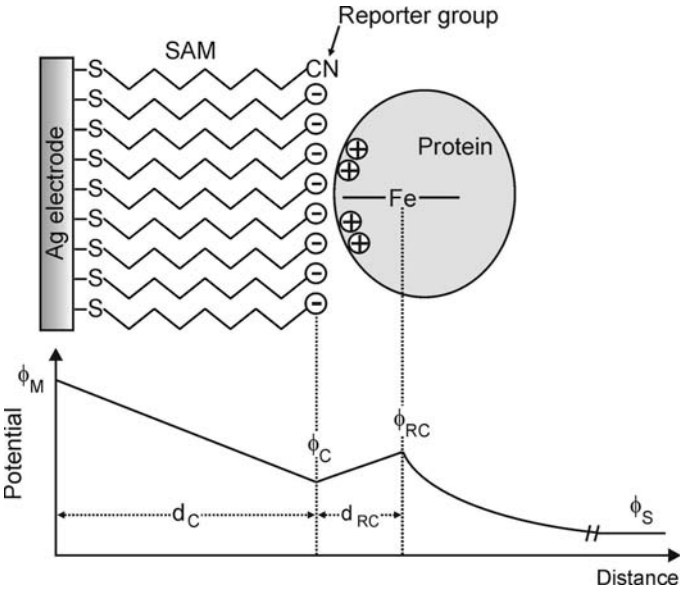

Fig. 4. Schematic representation of the interfacial potential distribution for Cyt-c electrostatically adsorbed on an Ag electrode coated with a COOH-terminated SAM

The interfacial potential distribution across the electrode/SAM/protein/solution interface can be described in terms of electrostatic theory as schematically shown in Fig. 4 [41]. The local electric-field at the protein binding site is controlled via the chain length and the tail functional group of the SAM, the electrode potential, and the pH and ionic strength of the solution. The predictions for SAMs of carboxylate-terminated thiols on Ag indicate local electric-field strengths at the SAM surface that are of the order 0.1 V/nm to 1 V/nm, and are, therefore, comparable to the values expected in the vicinity of charged phospholipid head groups of biological membranes [45].

Local electric-field strengths can also be determined experimentally by utilizing the vibrational Stark effect of appropriate reporter groups that are incorporated in the SAMs. For the nitrile function, the electric-field dependence of the vibrational frequency has been analyzed in detail by *Boxer* and coworkers [46, 47, 48]. On the basis of these results, determination of the C–N stretching frequency in SAMs including nitrile-terminated thiols by SER and SEIRA spectroscopy allows an estimation of the electric-field strength in the SAM/solution interface to be obtained (Fig. 4). Recent studies by *Harris* and coworkers and in our lab have shown that this approach provides results that are in good agreement with the values obtained by electrostatic theory [49, 50].

3 Electric-Field Effects on the Interfacial Processes of Heme Proteins

Electric-field strengths between 0.1 V/nm and 1 V/nm are sufficiently strong to alter protonation equilibria in proteins, to align and to induce molecular dipoles, to cause a redistribution of ions and solvent molecules, and even to perturb molecular energy levels [46]. These primary effects are likely to have consequences for the protein structure and the thermodynamics and kinetics of interfacial processes particularly when charge-transfer processes or changes of dipoles moments are involved.

3.1 Conformational Changes of Cytochrome c

Cyt-c is a small soluble monoheme protein that possesses a well-defined patch of positively charged lysine residues around the partially exposed heme edge that serves as the binding domain to its membrane-bound partner proteins [51]. Thanks to the heterogeneous distribution of surface charges and the resulting large dipole moment [52], it binds to negatively charged surfaces with high affinity and a largely uniform orientation. The binding domain of Cyt-c is likely to be the same for immobilization to electrodes coated with anionic SAMs as for complex formation with the natural reaction partners CcO or cytochrome c reductase. The SERR spectra of Cyt-c adsorbed to SAMs of carboxylate-terminated alkylthiols (C_n-SAMs with "n" denoting the number of methylen groups) on Ag with $n \geqslant 10$ are identical to the RR spectra in solution [41]. Also, the peak positions in the "reduced-minus-oxidized" IR difference spectra (SEIRA) obtained for Cyt-c adsorbed on Au coated with these C_n-SAMs and for the dissolved protein agree very well [10, 53, 54]. Furthermore, the redox potentials determined for the immobilized Cyt-c by SERR and SEIRA spectroscopy and corrected for the interfacial potential drop (see Sect. 3.2) were found to be the same as in solution. Thus, both the heme pocket and protein secondary structure remain unaffected upon adsorption under these conditions.

On the other hand, the SERR and SEIRA spectra of Cyt-c measured on shorter C_n-SAMs ($n < 10$) reveal additional contributions from non-native species denoted as B2 conformational state [41]. Similar B2 species have also been observed for electrostatic complexes of Cyt-c with micelles, phospholipid vesicles and polyanions in solution. The soluble complexes have been studied by a variety of spectroscopic methods, which revealed that the formation of the B2 state is associated with changes of the tertiary structure and the loss of the native axial ligand Met-80 [40,55,56,57]. This coordination site remains either vacant (five-coordinated high spin; 5cHS) or is occupied by a histidine residue (six-coordinated low spin; 6cLS), which has been identified as His-33 or His-26 (Fig. 5a). The transition from the native state B1 to the B2 state is reversible and involves the movement of the peptide segment 30(20)-49 to bring His-33 (His-26) into proximity with the heme iron.

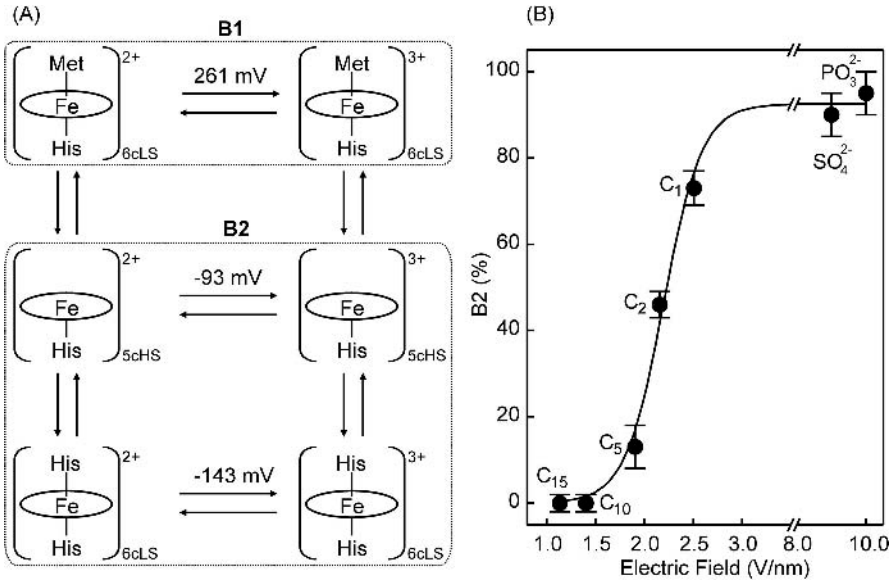

Fig. 5. (**a**) Schematic representation of the redox and conformational equilibria of Cyt-c in complexes with model systems. (**b**) Variation of the total amount of the B2 species of Cyt-c on electrodes with different coatings as a function of the electric field. See text for details

Formation of B2 is favored in the oxidized state due to the intrinsically lower stability of the Fe–Met bond in the ferric as compared to the ferrous form. On short C_n-SAMs, the B2 species can therefore only be observed for the ferric protein and reduction leads to the complete (re-)conversion to the B1 form [41]. The total amount of B2 species measured at the redox potential of the native state B1 shows a steady increase from 0 % at $n = 15$ and 10 up to 75 % at $n = 1$. This shift of the B2/B1 equilibrium is attributed to the increasing electric-field strength upon decreasing the SAM thickness. In agreement with this interpretation, a further increase of the electric field, which is achieved by coating the Ag with SAMs of phosphonate-terminated alkylthiols or with specifically adsorbed sulfate ions, shifts the conformational equilibrium almost completely towards B2 (Fig. 5b) [58]. At these latter two coatings, the electric-field is sufficiently strong to destabilize the Fe–Met bond also in the ferrous form. On sulfate-coated electrodes it was, therefore, possible to probe the redox equilibria of the B2 species leading to redox potentials of ca. −0.09 V and −0.14 V for the 5cHS and 6cLS couple, respectively [59]. This ca. 400 mV downshift of the redox potentials compared to the native B1 state can be readily attributed to the ligation and spin-state change as well as to the perturbation of the heme pocket structure.

A conformational transition to a B2-like conformational state is also observed upon hydrophobic binding both in solution (e.g., monomeric sodium

dodecyl sulfate) [40, 55, 56] or on electrodes covered with CH_3-terminated SAMs [22]. Hydrophobic interactions primarily lead to the displacement of the peptide segment 81–85 that is directly linked to the Met-80 and thus may cause the dissociation of this ligand from the heme. This segment is located in the center of the ring-like arrangement of lysine residues that are involved in electrostatic binding to anionic surfaces, implying that both modes of binding not only cause the same changes in the ligation pattern of the heme but also lead to approximately the same gross orientation of the protein with respect to the surface.

In contrast to the striking similarities of the kind of conformational changes, electrostatic and hydrophobic binding are associated with dramatic differences in the dynamics of the conformational transitions as probed in TR SERR experiments. Upon electrostatic binding the B1 → B2 transition occurs on the timescale of seconds but the rate increases by ca. five orders of magnitude for hydrophobically adsorbed Cyt-c [22, 58, 59].

3.2 Modulation of Redox Potentials

Potential-dependent SERR and SEIRA measurements of Cyt-c on C_n-SAMs indicate small downshifts of the measured redox potential upon increasing the chain length from $n = 1$ to 15 [41]. On the basis of electrostatic theory, these shifts can be quantitatively ascribed to the potential drops at the electrode/SAM/protein interfaces and thus do not reflect an alteration of the redox potential of the heme. Cyt-c immobilized on electrodes coated with polyelectrolyte multilayers, however, displays a different picture since the observed negative shifts of the redox potentials are larger by up to a factor of five [28]. Such electrode coatings are obtained by sequential adsorption of polycations (poly[ethylene imine] – PEI; polyallylamine hydrochloride – PAH) and polyanions (poly[styrene sulfonate] – PSS). Efficient Cyt-c binding only occurs when the terminating layer is PSS, which forms tight complexes with the cationic Cyt-c. In these complexes, ca. 40 % of the Cyt-c molecules are converted to the B2 state. However, the high negative charge density that is provided by the surrounding sulfonate groups also affects the remaining native state B1 by destabilizing the ferrous form such that the redox potential is lowered by more than 200 mV. This shift is not associated with structural changes of the heme site implying a direct perturbation of the redox potential by the electric-field.

This electric-field dependent modulation of the redox potential has been studied in detail in the case of the tetraheme cytochrome c_3 (Cyt-c_3), a small soluble electron/proton shuttle in the respiratory chain of *Desulfovibrio gigas* [17]. NMR studies of Cyt-c_3 in solution have revealed reduction potentials that increase in the order heme I (−287 mV), heme II (−279 mV), heme III (−262 mV) and heme IV (−183 mV) [60]. When electrostatically adsorbed to Ag electrodes coated with C_{10}-SAM, the SERR spectra of both the fully

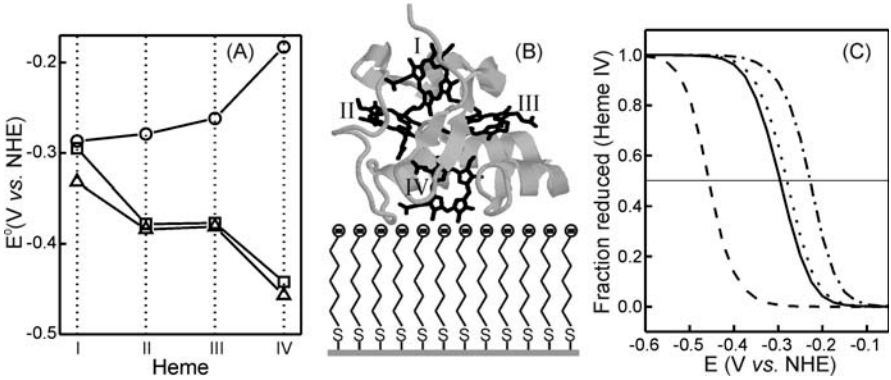

Fig. 6. (**a**) Reduction potentials for the individual hemes of Cyt-c_3 under different conditions. *Circles:* NMR titration in solution. *Squares:* SERR titration for Cyt-c_3 on an Ag electrode coated with C_{10}-SAM at pH 7. *Triangles:* theoretical prediction for Cyt-c_3 on a C_{10}-SAM at pH 7. (**b**) Orientation of Cyt-c_3 on a C_{10}-SAM as determined by molecular dynamics simulations. (**c**) Theoretical titration of heme IV of Cyt-c_3 computed under different conditions. *Dashed line:* charged C_{10}-SAM (pH 7). *Solid line:* solution. *Dotted line:* after removal of the C_{10}-SAM. *Dashed-dotted line:* neutral C_{10}-SAM

oxidized and fully reduced sample do not differ from the respective RR spectra in solution, suggesting that the protein retains its native structure upon immobilization. Electrochemical SERR titrations, however, indicate that the reduction potentials of the individual hemes are substantially downshifted with respect to the values in solution (Fig. 6a) such that the order of reduction is reversed with heme IV having the most negative redox potential (−390 mV), followed by heme III (−350 mV), heme II (−350 mV) and heme I (−270 mV).

Molecular dynamics simulations confirm that Cyt-c_3 docks to the C_{10}-SAM via the lysine-rich patch around heme IV under preservation of the protein structure (Fig. 6b). The redox potential shifts of the individual hemes determined in the SERR experiments are well reproduced by electrostatic calculations, with the largest downshift predicted for heme IV (161 mV) that is in closest contact to the anionic SAM surface. Electrostatic calculations performed on the structure optimized for the immobilized Cyt-c_3 but in the absence of the charged SAM yield redox potentials very similar to those calculated for the protein in solution (Fig. 6c). The calculations further predict a positive shift of the redox potentials for Cyt-c_3 immobilized on a fully neutralized SAM [17]. These results suggest that the redox potentials of the bound Cyt-c_3 are controlled by the interplay of two effects that tend to shift the redox potentials in opposite directions. On the one hand, the distance dependent electrostatic interactions between the individual hemes and the carboxylate groups of the SAM stabilize the oxidized forms, specifically of

heme IV that is in direct contact with the SAM, and, to a much lesser extent, of the more remote hemes. On the other hand, the low dielectric constant of the SAM with respect to the bulk aqueous medium tends to destabilize the formally monopositive ferric forms with respect to the formally neutral ferrous hemes.

A similar explanation holds for the behavior observed for cytochrome $P450_{cam}$ on Ag electrodes coated with C_n-SAMs of variable chain lengths [19]. SERR spectroscopy indicates that upon immobilization this enzyme does not retain the thiolate axial ligand and instead a P420 species is formed that is spectroscopically similar to the pressure-induced P420 in solution. The redox potential of P420 immobilized on a C_{15}-SAM is ca. 400 mV more positive than in solution but it shows a continuous downshift upon increasing the electric-field strength through shortening the chain length of the SAM or increasing the negative charge density on the electrode coating.

3.3 Electron-Transfer Dynamics of Cytochrome c and Other Soluble Electron Carriers

The heterogeneous electron-transfer (ET) of redox proteins immobilized on SAM-coated electrodes is expected to occur in the nonadiabatic regime due to the large separation between the redox center and the metal surface. Under these conditions, the formal ET rate constant $k_{ET}(0)$ is controlled by the weak electronic coupling that decays exponentially with the distance [61]:

$$k_{ET}(0) \propto H^0 \exp[-\beta(x - x_0)] , \tag{1}$$

where H^0 is the electronic coupling at the distance of closest approach x_0 and β is the tunneling decay parameter.

The distance dependence of $k_{ET}(0)$ has been studied for a number of proteins immobilized on Ag and Au electrodes coated with different types of SAMs, using a variety of electrochemical and spectroelectrochemical methods, including TR SERR [11, 16, 62, 63, 64, 65, 66]. A graphical summary for representative examples of these investigations is presented in Fig. 7a. At sufficiently long SAMs, the measured apparent rate constant $k_{app}(0)$, for all proteins exhibits the behavior predicted by (1) with approximately the same value for β corresponding to ca. 1.1 per CH_2 group, consistent with a redox reaction controlled by long-range tunneling. In contrast, $k_{app}(0)$ becomes distance independent at shorter SAMs suggesting either a change of mechanism or the coupling of ET with another process that becomes rate limiting.

For Cyt-c on a C_{15}-SAM the reduction rate shows a clear overpotential dependence, which can be treated according to Marcus-DOS theory for nonadiabatic ET reactions (Fig. 7b) yielding a reorganization energy $\lambda = 0.24$ eV [67, 68]. This value, which was also confirmed by temperature-dependent measurements of $k_{ET}(0)$, is distinctly lower than that determined for Cyt-c in solution (ca. 0.6 eV). The discrepancy can be understood taking

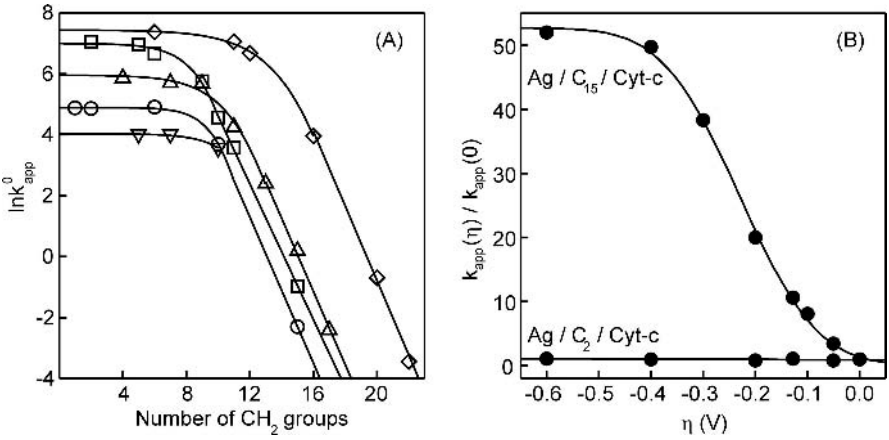

Fig. 7. (**a**) Distance dependence of the apparent ET rate for different systems. *Down-triangles:* cytochrome b_{562} on Ag coated with NH_2-terminated SAMs [16]. *Circles:* Cyt-c on Ag coated with COOH-terminated SAMs [62]. *Up-triangles:* azurin on Au coated with CH_3-terminated SAMs [11]. *Squares:* Cyt-c on Au coated with COOH-terminated SAMs [63]. *Diamonds:* Cyt-c on Au coordinatively bound to pyridine-terminated SAMs [64, 65, 66]. (**b**) Overpotential dependence of the apparent ET rate for Cyt-c on Ag electrodes coated with two different COOH-terminated SAMs

into account that the largest contribution to the reorganization energy results from the solvent and protein matrix rearrangement [69, 70]. In the adsorbed state, solvent reorganization is likely to be reduced as compared to the solution due to the exclusion of water molecules from the binding domain and due to the lower dielectric constant, which is presumably smaller than 10 in the electrochemical interface compared to 78 in the bulk solution.

On the other hand, the measured rate for Cyt-c on a C_1- or C_2-SAM is independent of the overpotential, indicating that at shorter distances ET does not constitute the rate-limiting step [58, 67]. In this region, $k_{app}(0)$ decreases upon increasing the viscosity of the solution as determined by TR SERR and electrochemical techniques [58, 63]. *Avila* et al. [63] proposed a reaction scheme that involves the adsorption of Cyt-c in a thermodynamically stable orientation that is redox-inactive and requires a transient reorientation before electron tunneling can take place. Since only the latter step is distance dependent, the overall reaction rate reaches a limiting value when ET approaches the rate of the distance independent reorientation. However, this model cannot account for all experimental observations, like the decrease of the apparent ET rate observed upon H_2O/D_2O exchange, which originally was attributed to proton-transfer steps becoming rate limiting [62]. The increasing ratio of the rate constants measured in H_2O and D_2O from 1.0 at C_{15}-SAMs to 4.0 at C_1-SAMs can be reinterpreted in terms of the ca. 20 % higher viscosity of D_2O with respect to H_2O; but it remains puzzling why the

apparent rate constant in H_2O is constant at C_n-SAMs with $n < 10$ while it decreases in D_2O.

On the other hand, reorientation of Cyt-c must involve the rupture and formation of salt bridges between the protein surface and the electrode coating, and thus should be affected by the charge densities of the protein and the C_n-SAM as well as by the realignment of the protein dipole moment in the interfacial electric-field. Both the charge density of the C_n-SAM and the strength of the interfacial electric-field increase at short chain lengths such that protein reorientation should be slowed down when the field becomes sufficiently strong.

This prediction was in fact confirmed in TR SERR experiments with Cyt-c immobilized on Ag electrodes covered with specifically adsorbed sulfate ions and phosphonate-terminated SAMs [58, 59]. Although the strong electric-fields at these coatings lead to a substantial portion of the B2 state (vide supra) and even cause a slow irreversible denaturation, TR SERR still allows determination of the apparent ET rate for the fraction of immobilized protein that remains in the native state B1. The measured rates for Cyt-c adsorbed on SO_4–Ag and PO_3–SAM are significantly lower than for C_n-SAMs at comparable distances. Indeed, a plot of the apparent rates as a function of the electric-field strength (Fig. 8) yields a uniform picture for all the different coatings consistent with a heterogeneous redox reaction that is controlled by electron tunneling at long distances and by electric-field-dependent reorientation at short distances. Qualitatively similar results were obtained for cytochrome c_6 (Cyt-c_6), a soluble monoheme protein that acts as an electron carrier between the b_6f complex and photosystem I (PSI) in photosynthetic redox chains [20].

A different mechanism holds, however, for Cyt-c that is attached to the electrode via coordination of the heme iron by the tail group of pyridinyl-terminated SAM [24, 25, 26, 64, 65, 71]. Also in this case, the experimentally determined rate constants approach a limiting value at short distances and then become viscosity dependent. However, in contrast to electrostatic adsorption, the ET rate constant in the distance independent regime exhibits a strong increase with the overpotential [72]. This behavior is consistent with an adiabatic or friction-controlled ET mechanism, as originally suggested by *Waldeck* and coworkers [25, 26, 64, 65, 71].

3.4 Electric-Field Effects on the Electroprotonic Energy Transduction of Heme-Cu Oxidases

Heme-Cu oxidases constitute a superfamily of terminal enzymes in respiratory chains that catalyze the reduction of molecular oxygen to water and use the energy provided by exergonic electron-transfer events to pump protons trough the membrane against a gradient [73, 74]. The best-known members of this group of enzymes are the mitochondrial-type CcOs in which a binuclear

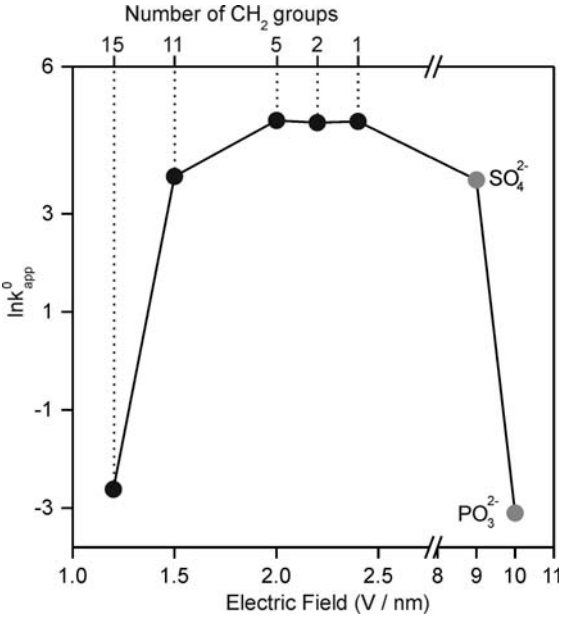

Fig. 8. Electric-field dependence of the apparent ET rate constant of Cyt-c on coated Ag electrodes. The *black points* represent COOH-terminated SAMs of different chain lengths. The *gray points* refer to Ag coated with either specifically adsorbed sulfate anions or with 11-thioundecyl-1-phosphonic acid

center, a high-spin heme a_3 and a copper B center (Cu_B), constitute the catalytic site. The entry site for the electrons delivered by Cyt-c is a binuclear copper A center (Cu_A) from which the electrons are further transferred to a low-spin heme a and subsequently to the catalytic site where bound oxygen is reduced.

We have recently studied CcO integrated into a lipid bilayer and anchored to a Ni(Zn)–NTA-coated electrode via a his-tag introduced at the C-terminus of either subunit I or II, such that the primary electron acceptor, the Cu_A site, is either facing the electrode or the solution, respectively [35, 37]. The immobilized enzymes retain the native structure at the level of the hemes a and a_3 as judged from the SERR spectra that do not differ from the corresponding RR spectra in solution. In both orientations the immobilized CcO can be reversibly reduced and oxidized under anaerobic conditions, as indicated by the potential-dependent changes of the oxidation marker bands (Fig. 9). However, a careful inspection of the SERR spectra in the $1500\,cm^{-1}$ to $1700\,cm^{-1}$ region demonstrates that only heme a is redox-active, while heme a_3 remains oxidized even at $-0.45\,V$, that is at very negative overpotentials.

The heterogeneous ET rate constant was found to be nearly identical for both orientations, ca. $0.002\,s^{-1}$, and independent of the electrode potential

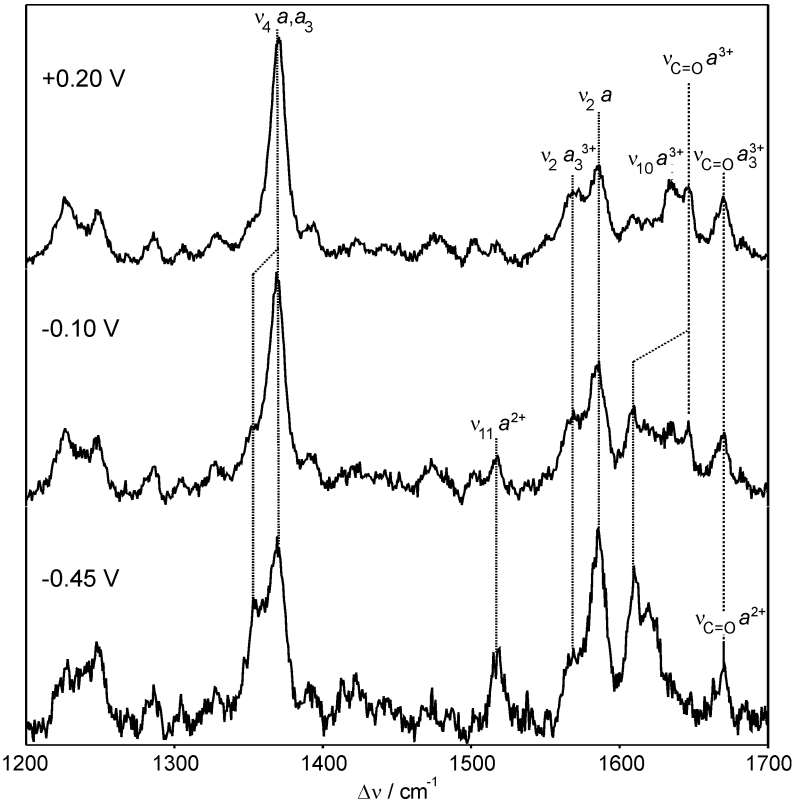

Fig. 9. Potential dependence of the SERR spectra of CcO immobilized on Ag electrodes using the Ni–NTA/his-tag approach. See text for details

between 200 mV and −160 mV. Thus, it was concluded that the natural electron entry site, i.e., the Cu_A center, does not participate in the electronic pathways involved in this model system. The through-space distance from the electrode surface to heme *a* is ca. 50 Å in both CcO orientations. For such long distances, electron tunneling is highly unlikely and cannot be reconciled with a rate constant of $0.002\,s^{-1}$. Most likely the redox mechanism involves multistep electron tunneling or hopping via the amide functions of the NTA spacer and the polypeptide backbone as proposed by *Morita* and *Kimura* for helical peptides [75].

Irrespective of the details of the mechanism of electronic communication between the electrode and heme *a* in this artificial system, it is particularly remarkable that heme a_3 is not reduced. Intramolecular ET from heme *a* to heme a_3 is expected to occur within nanoseconds [76] despite the fact that, in the fully oxidized state, the midpoint potentials of hemes *a* and a_3 of mammalian CcO are ca. +390 mV and +200 mV, respectively, which in principle

would correspond to an uphill electron-transfer process. However, the midpoint potentials of the four redox centers in CcO are strongly modulated by the respective oxidation states and the protonation state of redox-Bohr sites. The underlying molecular mechanism that ensures an efficient downhill electron-transfer cascade coupled to uphill proton translocation is still a matter of debate, but it essentially consists of a complex network of cooperativities, including Coulombic interactions and mechanochemical components [77,78,79]. The failure to reduce heme a_3 in the immobilized CcO, directly through the electrode or via intramolecular ET from heme *a*, suggests that the internal H^+/e^- cooperativity network is disturbed possibly due to electric-field-induced alterations of pK_as such that crucial proton-transfer steps coupled to the ET reactions are blocked or slowed down.

Indirect evidence for electric-field-induced perturbation of proton-transfer events has also been obtained for the quinol oxidaze (QO) from *A. ambivalens* [31]. Like CcO, this enzyme contains a Cu_B-heme a_3 binuclear active center and a heme *a* as its immediate electron donor, but instead of a Cu_A a loosely bound quinone acts as the electron-entry site [80]. The direct adsorption of detergent-solubilized QO to a "bare" Ag electrode occurs without displacement of the detergent that, hence, acts as a biocompatible interface. Indeed, the peak positions in the SERR spectra of the solubilized enzyme are identical to those in the RR spectra of QO in solution, indicating that the structures of the heme pockets are largely preserved [31]. Unlike CcO, potential-dependent SERR measurements of the immobilized QO clearly reveal a reversible electrochemistry for both hemes. Moreover, the spectral-component analysis yields nearly ideal Nernstian plots (Fig. 10) pointing to rather weak Coulombic interactions between the redox centers of QO that is also in sharp contrast to mitochondrial CcO. The redox potentials determined in the SERR experiments are +320 mV and +390 mV for hemes *a* and a_3, respectively, and thus are in the reversed order with respect to CcO. Both the reversed order of redox potentials as well as the lack of substantial Coulombic interactions represent a unique case among the superfamily of oxygen reductases. While CcO requires a complex network of cooperativity effects to guarantee a downhill ET sequence, the exergonicity in QO is already ensured by its inverted redox potentials.

Reduction of heme a_3 of QO in solution is followed by a weakening of the hydrogen-bond interactions of the formyl substituent as reflected by the frequency shift of the C=O stretching from 1661 cm^{-1} to 1669 cm^{-1} in the RR spectrum [80]. This process is believed to constitute a key step in the proton-pumping activity of the enzyme. On the other hand, the SERR spectrum of the reduced immobilized QO only displays the band at 1661 cm^{-1} and no time-dependent increase of intensity at 1669 cm^{-1} is noted within 30 min, implying that the redox-linked reorganization of the hydrogen-bond interactions in the catalytic center is blocked or at least drastically slowed down in the presence of high electric fields [31].

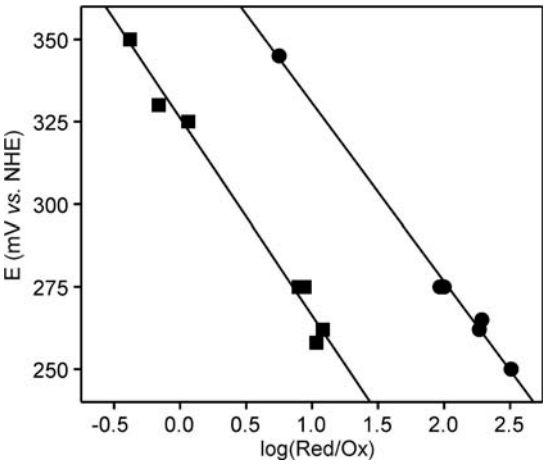

Fig. 10. Nernstian plots for the two hemes of QO immobilized on detergent-coated Ag electrodes. *Squares:* heme *a*. *Circles:* heme a_3

4 Concluding Remarks

Surface-enhanced vibrational spectroelectrochemistry constitutes a powerful approach for elucidating the reaction mechanisms and dynamics of immobilized redox proteins. In contrast to traditional electrochemical methods, the combination of SERR and SEIRA provides a direct and detailed molecular picture of all potential-dependent processes of the adsorbed species, including those that are non-Faradaic reactions. In this respect, these techniques may gain increasing importance in both fundamental and applied science. On the one hand, a profound knowledge of the molecular structure and dynamics of immobilized proteins and enzymes that can be obtained by these methods is a prerequisite for the rational design of bioelectronic devices of technological importance. On the other hand, surface-enhanced vibrational spectroscopies open new possibilities to study complex biomimetic systems, thereby providing novel insight into fundamental biological processes.

In this contribution we have presented a simple way for studying the influence of electric-fields on the various parameters that control electron-and proton-transfer reactions of soluble and membrane-bound proteins like Cyt-c and CcO. We have shown that electric fields of a magnitude comparable to those at the interfaces of biomembranes, i.e., the natural reaction environment, may have a substantial influence on redox potentials, protein structure, redox-linked conformational changes and orientation/reorientation of electrostatic complexes. These studies do not directly prove a functional role of the electric-field effects in vivo, but they clearly indicate that such effects might be present and deserve further investigation. The application of surface-enhanced vibrational spectroscopic methods in combination with more realistic model systems appears to be a promising strategy towards that goal.

References

[1] T. M. Cotton, S. G. Schultz, R. P. Van Duyne: J. Am. Chem. Soc. **102**, 7960 (1980)
[2] K. M. Ervin, E. Koglin, J. M. Sequaris, P. Valenta, H. W. Nurnberg: J. Electroanal. Chem. **114**, 179 (1980)
[3] R. E. Holt, T. M. Cotton: J. Am. Chem. Soc. **111**, 2815 (1989)
[4] G. Smulevich, T. G. Spiro: J. Phys. Chem. **89**, 5168 (1985)
[5] D. H. Murgida, P. Hildebrandt: Acc. Chem. Res. **37**, 854 (2004)
[6] D. H. Murgida, P. Hildebrandt: Phys. Chem. Chem. Phys. **7**, 3773 (2005)
[7] C. T. Shi, Z. Wei, R. L. Birke, J. R. Lombardi: J. Phys. Chem. **94**, 4766 (1990)
[8] D. H. Murgida, P. Hildebrandt: Angew. Chem. Int. Ed. **40**, 728 (2001)
[9] H. Wackerbarth, U. Klar, W. Gunther, P. Hildebrandt: Appl. Spectrosc. **53**, 283 (1999)
[10] K. Ataka, J. Heberle: J. Am. Chem. Soc. **125**, 4986 (2003)
[11] Q. J. Chi, J. D. Zhang, J. E. T. Andersen, J. Ulstrup: J. Phys. Chem. B **105**, 4669 (2001)
[12] N. Mohtat, M. Byloos, M. Soucy, S. Morin, M. Morin: J. Electroanal. Chem. **484**, 120 (2000)
[13] K. Shimazu, T. Kawaguchi, T. Isomura: J. Am. Chem. Soc. **124**, 652 (2002)
[14] C. A. Widrig, C. Chung, M. D. Porter: J. Electroanal. Chem. **310**, 335 (1991)
[15] M. Schweizer, H. Hagenstrom, D. M. Kolb: Surf. Sci. **490**, L627 (2003)
[16] T. Albrecht, P. D. Barker, D. H. Murgida, P. Hildebrandt: unpublished results
[17] L. Rivas, C. M. Soares, A. M. Baptista, J. Simaan, R. D. Paolo, D. H. Murgida, P. Hildebrandt: Biophys. J. **88**, 4188 (2005)
[18] A. J. Simaan, D. H. Murgida, P. Hildebrandt: Biopolymers **67**, 331 (2002)
[19] S. Todorovic, C. Jung, P. Hildebrandt, D. H. Murgida: J. Biol. Inorg. Chem. **11**, 119 (2006)
[20] A. Kranich, M. A. De la Rosa, P. Hildebrandt, D. H. Murgida: unpublished results
[21] D. H. Murgida, P. Hildebrandt: J. Mol. Struct. **565**, 97 (2001)
[22] L. Rivas, D. H. Murgida, P. Hildebrandt: J. Phys. Chem. B **106**, 4823 (2002)
[23] L. J. C. Jeuken, J. P. Mcevoy, F. A. Armstrong: J. Phys. Chem. B **106**, 2304 (2002)
[24] D. H. Murgida, P. Hildebrandt, J. Wei, Y. F. He, H. Y. Liu, D. H. Waldeck: J. Phys. Chem. B **108**, 2261 (2004)
[25] J. J. Wei, H. Y. Liu, A. R. Dick, H. Yamamoto, Y. F. He, D. H. Waldeck: J. Am. Chem. Soc. **124**, 9591 (2002)
[26] H. Yamamoto, H. Y. Liu, D. H. Waldeck: Chem. Commun. p. 1032 (2001)
[27] I. Willner, V. HelegShabtai, R. Blonder, E. Katz, G. L. Tao: J. Am. Chem. Soc. **118**, 10321 (1996)
[28] I. Weidinger, D. H. Murgida, W. F. Dong, H. Möhwald, P. Hildebrandt: J. Phys. Chem. B **110**, 522 (2006)
[29] M. K. Beissenhirtz, F. W. Scheller, F. Lisdat: Anal. Chem. **76**, 4665 (2004)
[30] M. K. Beissenhirtz, F. W. Scheller, W. F. M. Stocklein, D. G. Kurth, H. Mohwald, F. Lisdat: Angew. Chem. Int. Ed. **43**, 4357 (2004)
[31] S. Todorovic, M. M. Pereira, T. M. Bandeiras, M. Teixeira, P. Hildebrandt, D. H. Murgida: J. Am. Chem. Soc. **127**, 13561 (2005)

[32] J. A. He, L. Samuelson, L. Li, J. Kumar, S. K. Tripathy: Adv. Mater. **11**, 435 (1999)
[33] W. M. Mirsky (Ed.): *Ultrathin Electrochemical Chemo- and Biosensors, Technology and Performance* (Springer, Berlin, Heidelberg 2004)
[34] K. Ataka, F. Giess, W. Knoll, R. Naumann, S. Haber-Pohlmeier, B. Richter, J. Heberle: J. Am. Chem. Soc. **126**, 16199 (2004)
[35] M. G. Friedrich, F. Giess, R. Naumann, W. Knoll, K. Ataka, J. Heberle, J. Hrabakova, D. H. Murgida, P. Hildebrandt: Chem. Commun. p. 2376 (2004)
[36] F. Giess, M. G. Friedrich, J. Heberle, R. L. Naumann, W. Knoll: Biophys. J. **87**, 3213 (2004)
[37] J. Hrabakova, K. Ataka, J. Heberle, P. Hildebrandt, D. H. Murgida: Phys. Chem. Chem. Phys. **8**, 759 (2006)
[38] E. Sackmann: Science **271**, 43 (1996)
[39] S. Z. Hu, I. K. Morris, J. P. Singh, K. M. Smith, T. G. Spiro: J. Am. Chem. Soc. **115**, 12446 (1993)
[40] S. Oellerich, H. Wackerbarth, P. Hildebrandt: J. Phys. Chem. B **106**, 6566 (2002)
[41] D. H. Murgida, P. Hildebrandt: J. Phys. Chem. B **105**, 1578 (2001)
[42] S. Döpner, P. Hildebrandt, A. G. Mauk, H. Lenk, W. Stempfle: Spectrochim. Acta Part A: Mol. Biomol. Spectrosc. **52**, 573 (1996)
[43] P. Hildebrandt, M. Stockburger: Biochem. **28**, 6710 (1989)
[44] A. Bonifacio, D. Millo, C. Gooijer, R. Boegschoten, G. van der Zwan: Anal. Chem. **76**, 1529 (2004)
[45] R. J. Clarke: Adv. Coll. Int. Sci. **89**, 263 (2001)
[46] I. T. Suydam, S. G. Boxer: Biochem. **42**, 12050 (2003)
[47] S. S. Andrews, S. G. Boxer: J. Phys. Chem. A **106**, 469 (2002)
[48] S. S. Andrews, S. G. Boxer: J. Phys. Chem. A **104**, 11853 (2000)
[49] V. Oklejas, C. Sjostrom, J. M. Harris: J. Phys. Chem. B **107**, 7788 (2003)
[50] V. Oklejas, J. M. Harris: Langmuir **19**, 5794 (2003)
[51] R. A. Scott, A. G. Mauk (Eds.): *Cytochrome c - A Multidisciplinary Approach* (University Science Books, Sausalito 1995)
[52] W. H. Koppenol, J. D. Rush, J. D. Mills, E. Margoliash: Mol. Biol. Evol. **8**, 545 (1991)
[53] K. Ataka, J. Heberle: J. Am. Chem. Soc. **126**, 9445 (2004)
[54] N. Wisitruangsakul, I. Zebger, P. Hildebrandt, D. H. Murgida: unpublished results
[55] S. Oellerich, H. Wackerbarth, P. Hildebrandt: Eur. Biophys. J. Biophys. Lett. **32**, 599 (2003)
[56] S. Oellerich, S. Lecomte, M. Paternostre, T. Heimburg, P. Hildebrandt: J. Phys. Chem. B **108**, 3871 (2004)
[57] H. Wackerbarth, D. H. Murgida, S. Oellerich, S. Dopner, L. Rivas, P. Hildebrandt: J. Mol. Struct. **563**, 51 (2001)
[58] L. Rivas, M. Marti, P. Hildebrandt, D. H. Murgida: unpublished results
[59] H. Wackerbarth, P. Hildebrandt: Chem. Phys. Chem. **4**, 714 (2003)
[60] R. O. Louro, T. Catarino, D. L. Turner, M. A. Picarra-Pereira, I. Pacheco, J. LeGall, A. V. Xavier: Biochem. **37**, 15808 (1998)
[61] A. M. Kuznetsov, J. Ulstrup: *Electron Transfer in Chemistry and Biology. An Introduction to the Theory* (Wiley, Chichester 1999)
[62] D. H. Murgida, P. Hildebrandt: J. Am. Chem. Soc. **123**, 4062 (2001)

[63] A. Avila, B. W. Gregory, K. Niki, T. M. Cotton: J. Phys. Chem. B **104**, 2759 (2000)
[64] D. E. Khoshtariya, J. J. Wei, H. Y. Liu, H. J. Yue, D. H. Waldeck: J. Am. Chem. Soc. **125**, 7704 (2003)
[65] J. J. Wei, H. Y. Liu, D. E. Khoshtariya, H. Yamamoto, A. Dick, D. H. Waldeck: Angew. Chem. Int. Ed. **41**, 4700 (2002)
[66] J. J. Wei, H. Y. Liu, K. Niki, E. Margoliash, D. H. Waldeck: J. Phys. Chem. B **108**, 16912 (2004)
[67] P. Hildebrandt, D. H. Murgida: Bioelectrochem. **55**, 139 (2002)
[68] D. H. Murgida, P. Hildebrandt: J. Phys. Chem. B **106**, 12814 (2002)
[69] G. Basu, A. Kitao, A. Kuki, N. J. Go: J. Phys. Chem. B **102**, 2085 (1998)
[70] I. Muegge, P. X. Qi, A. J. Wand, Z. T. Chu, A. Warshel: J. Phys. Chem. B **101**, 825 (1997)
[71] T. D. Dolidze, D. E. Khoshtariya, D. H. Waldeck, J. Macyk, R. van Eldik: J. Phys. Chem. B **107**, 7172 (2003)
[72] J. Hrabakova, Y. Hongjun, D. H. Waldeck, P. Hildebrandt, D. H. Murgida: unpublished results
[73] M. M. Pereira, M. Teixeira: Biochim. Biophys. Acta Bioenerg. **1655**, 340 (2004)
[74] M. M. Pereira, M. Santana, M. Teixeira: Biochim. Biophys. Acta Bioenerg. **1505**, 185 (2001)
[75] T. Morita, S. Kimura: J. Am. Chem. Soc. **125**, 8732 (2003)
[76] A. Jasaitis, F. Rappaport, E. Pilet, U. Liebl, M. H. Vos: Proc. Natl. Acad. Sci. USA **102**, 10882 (2005)
[77] M. Brunori, A. Giuffre, P. Sarti: J. Inorg. Biochem. **99**, 324 (2005)
[78] M. Wikstrom: Biochim. Biophys. Acta Bioenerg. **1655**, 241 (2004)
[79] A. V. Xavier: Biochim. Biophys. Acta Bioenerg. **1658**, 23 (2004)
[80] T. K. Das, C. M. Gomes, T. M. Bandeiras, M. M. Pereira, M. Teixeira, D. L. Rousseau: Biochim. Biophys. Acta Bioenerg. **1655**, 306 (2004)

Index